Available online at www.sciencedirect.com
SCIENCE DIRECT®
Journal of Computational Physics 207 (2005) 610–624
JOURNAL OF COMPUTATIONAL PHYSICS
www.elsevier.com/locate/jcp

A smoothed particle hydrodynamics model for miscible flow in three-dimensional fractures and the two-dimensional Rayleigh–Taylor instability

Alexandre M. Tartakovsky [a,*], Paul Meakin [b]

[a] *Pacific Northwest National Laboratory, P.O. Box 999/MS K1-85, Richland, WA 99352, USA*
[b] *Idaho National Engineering and Environmental Laboratory, P.O. Box 1625, MS 2025, Idaho Falls, ID 83415-2025, USA*

Received 16 April 2004; received in revised form 11 November 2004; accepted 1 February 2005
Available online 3 March 2005

Abstract

A numerical model based on smoothed particle hydrodynamics (SPH) has been developed and used to simulate the classical two-dimensional Rayleigh–Taylor instability and three-dimensional miscible flow in fracture apertures with complex geometries. To model miscible flow fluid particles with variable, composition dependent, masses were used. By basing the SPH equations on the particle number density artificial surface tension effects were avoided. The simulation results for the growth of a single perturbation driven by the Rayleigh–Taylor instability compare well with numerical results obtained by Fournier et al., and the growth of a perturbation with time can be represented quite well by a second-degree polynomial, in accord with the linear stability analysis of Duff et al. The dispersion coefficient found from SPH simulation of flow and diffusion in an ideal fracture was in excellent agreement with the value predicted by the theory of Taylor and Aris. The simulations of miscible flow in fracture apertures can be used to determination dispersion coefficients for transport in fractured media – a parameter used in large-scale simulations of contaminant transport.

Keywords: Smoothed particle hydrodynamics; Miscible flow; Rayleigh–Taylor instability; Flow and transport in fractures

1. Introduction

Miscible flow is a common and important phenomenon encountered in many areas of natural science and technology. Under the influence of gravity, the miscible flow of fluids with sufficiently large density

* Corresponding author. Tel.: +1 509 372 6185; fax: +1 509 375 6631.
E-mail addresses: alexandre.tartakovsky@pnl.gov (A.M. Tartakovsky), meakp@inel.gov (P. Meakin).

0021-9991/$ - see front matter
doi:10.1016/j.jcp.2005.02.001

ratios may become unstable, a process known as the Rayleigh–Taylor instability [1]. Examples of the Rayleigh–Taylor instability include supernova explosions [2], fire propagation in vertical shafts [3] and contaminant transport in porous media [4].

In a miscible flow, a single fluid phase is present but its composition and properties (e.g., density, chemical composition and temperature) vary in space. The fluid may be composed of two miscible fluids or a solute non-uniformly dissolved in a liquid [5]. The miscible flow of two fluids such as salty water and fresh water having a single fluid phase but different solute concentrations is addressed in this work. Miscible flow is governed by a combination of momentum and mass conservation equations that describe the flow of the fluid phase and a convection-diffusion equation describing the change of concentration in the fluid phase. When Rayleigh–Taylor or other instabilities develop it may be difficult to use standard grid-based methods to model miscible flow since the domains occupied by miscible fluids have very complex constantly changing geometries. Under these conditions, grid-based numerical methods often result in artificial numerical diffusion, the violation of mass conservation and grid entanglement. An alternative approach is to use particles to represent the fluids.

In this paper, a numerical model based on smoothed particle hydrodynamics (SPH) is used to simulate miscible flow. The application of the model to the classical two-dimensional Rayleigh–Taylor instability (the instability that develops when a layer of dense fluid lies initially above a layer of less dense fluid) and three-dimensional miscible flow in fracture apertures with complex geometries is described. Miscible flow in fractures plays an important role in the migration of contaminants in the subsurface. Flow in the shallow subsurface is often dominated by flow in fractures, and this may play an important role in the transport of dissolved contaminants in groundwater and the intrusion of seawater into aquifers.

SPH is an interpolation-based numerical technique that can be used to solve systems of partial differential equations. The Lagrangian particle nature of SPH allows physical and chemical effects to be incorporated into the modeling of flow processes with relatively little code-development effort. In addition, geometrically complex and/or dynamic boundaries and interfaces can be handled without undue difficulty. SPH was first introduced by Lucy [6] and Gingold and Monaghan [7] to simulate fluid dynamics in the context of astrophysical applications. Since its introduction, SPH has been successfully used to model a wide range of fluid flow processes and the behavior of solids subjected to large deformations. For example, Liu et al. [8] applied SPH to simulate high energy impacts and explosions, Monaghan [9] used SPH to model the collapse of dams, Morris, Fox and Zhu [10] extended SPH to model low Reynolds number flows, Zhu, Fox and Morris [11] applied SPH to study pore-scale flow, and Zhu and Fox [12,13] used SPH to model pore scale diffusion and dispersion.

Hoover [14] and Colagrossi and Landrini [15] used SPH to model the immiscible flow of two fluids and found that the standard SPH formulation of Gingold and Monaghan [7] creates artificial surface tension on the boundary between the two fluids. In this paper, we propose a modified form of the SPH flow equations that eliminates artificial surface tension. A combination of the modified SPH flow equation with an SPH advection-diffusion equation similar to that derived by Zhu and Fox [12,13] allows miscible flow to be realistically modeled.

2. SPH equations

In SPH, the fluid is represented by a discrete set of N particles. The position of the ith particles is denoted by the vector $\mathbf{r}_i$, $i = 1, \ldots, N$. SPH theory is based on the idea that a smoothed representation $A_S(\mathbf{r})$ of the continuous function $A(\mathbf{r})$ at position $\mathbf{r}$ can be found from:

$$A_S(\mathbf{r}) = \int A(\mathbf{r}')W(\mathbf{r} - \mathbf{r}\prime, h)\mathrm{d}\mathbf{r}', \tag{1}$$

where h is the support scale of the weighting function W, which satisfies the normalization condition

$$\int W(\mathbf{r}-\mathbf{r}',h)\mathrm{d}\mathbf{r}' = 1, \tag{2}$$

and the integration is performed over the entire space of the field. In the $h \to 0$ limit, the weighting function W becomes a Dirac delta function and $A_S(\mathbf{r}) \to A(\mathbf{r})$.

In standard SPH, the properties associated with any particle i are calculated by approximating the integral in (1) by the sum

$$A_i = um_j\Delta V_j A_j W(\mathbf{r}_i-\mathbf{r}_j,h) = \sum_j m_j \frac{A_j}{\rho_j} W(\mathbf{r}_i-\mathbf{r}_j,h), \tag{3}$$

where ΔV_j is the volume of fluid associated with particle j, and m_j and ρ_j are the mass and density of the jth particle. In this equation, A_j is the value of A at particle j, and the summation is performed over all of the particles. Similarly, the gradient of A is calculated from

$$\nabla A_i = \sum_j m_j \frac{A_j}{\rho_j} \nabla_i W(\mathbf{r}_i-\mathbf{r}_j,h), \tag{4}$$

and the magnitude of the field A at position $\mathbf{r}$ is approximated by

$$A(\mathbf{r}) = \sum_j m_j \frac{A_j}{\rho_j} W(\mathbf{r}-\mathbf{r}_j,h). \tag{5}$$

In Eq. (3), m_i/ρ_i can be replaced by the particle number density n_i, and Eq. (3) can be replaced by

$$A_i = \sum_j \frac{A_j}{n_j} W(\mathbf{r}_i-\mathbf{r}_j,h), \tag{6}$$

where n_i has units of (L^{-3}) and satisfies

$$n_i\Delta V_i \equiv 1. \tag{7}$$

The particle number density calculated from (6) is

$$n_i = \sum_j W(\mathbf{r}_i-\mathbf{r}_j,h), \tag{8}$$

and the mass density ρ_i obtained from (5) is

$$\rho_i = \sum_j m_i W(\mathbf{r}_i-\mathbf{r}_j,h). \tag{9}$$

Similarly, gradients are calculated from

$$\nabla A_i = \sum_j \frac{A_j}{n_j} \nabla_i W(\mathbf{r}_i-\mathbf{r}_j,h). \tag{10}$$

The motion of each particle is governed by momentum and mass (or particle number) conservation principles described by the Navier–Stokes equations. In standard SPH, expressions (3) and (4) are used to approximate the fields and spatial derivatives that enter into the Navier–Stokes equations, while in this work we use expressions (6) and (10). For simple one-phase flow, when all the particles are assumed to have the same time invariant mass, the same results are obtained using either n or ρ in the SPH equations. For multiphase flows and miscible multicomponent flows, such as the flow of fresh and salt water, it is important to distinguish between the mass and particle densities.

In miscible flows, the velocity field is governed by a momentum conservation equation with the form

$$\frac{\mathrm{d}(m_i(t,C)\mathbf{v}_i(t))}{\mathrm{d}t} = (-\nabla P_i(t) + \mu_i(C)\nabla^2\mathbf{v}_i(t))V_i(t,\rho_i) + m_i(t,C)\mathbf{g} \tag{11}$$

coupled with a convection-diffusion equation [13]

$$\frac{\mathrm{d}C_i(t)}{\mathrm{d}t} = D(\nabla^2 C(t))_i. \tag{12}$$

Here, $\mathbf{v}$ is the fluid velocity vector, P is the pressure, $\mathbf{g}$ is the gravitational acceleration vector, and μ is the dynamic viscosity of the solution, which generally depends on the solute concentration. In Eq. (11) the mass m_i of particle i depends on the solute concentration (or more generally on the composition of the fluid).

For salt solutions, the fluid volume does not increase significantly when the salt is added, and the density depends approximately linearly on the salt concentration, providing the concentration is not too high. In this work, a simple linear relationship between solution density and solute concentration was used, and this can be represented by the relationship

$$m_i = m_i^{\mathrm{f}} + kC_i, \tag{13}$$

between the mass m_i carried by particle i in the SPH model and the solute concentration C_i where k is a constant and m_i^{f} is the mass of the solvent carried by each particle. Under these conditions, the number density of the fluid is independent of the fluid composition.

Using the equivalence between the volume associated with a particle and the reciprocal of the number density (Eq. (7)), the momentum conservation equation can be rewritten as

$$\frac{\mathrm{d}(m_i(t,C)\mathbf{v}_i(t))}{\mathrm{d}t} = -\frac{1}{n_i}\nabla P_i(t) + \frac{\mu_i(C)}{n_i}\nabla^2\mathbf{v}_i(t) + m_i(t,C)\mathbf{g}. \tag{14}$$

In SPH, with particles of constant mass, the momentum conservation equation is

$$\frac{\mathrm{d}\mathbf{v}_i(t)}{\mathrm{d}t} = -\frac{1}{\rho_i}\nabla P_i(t) + \frac{\mu_i}{\rho_i}\nabla^2\mathbf{v}_i(t) + \mathbf{g} \tag{15}$$

and the most common SPH approximation of this equation is

$$\frac{\mathrm{d}\mathbf{v}_i}{\mathrm{d}t} = -\sum_j m_j\left(\frac{P_j}{\rho_j^2} + \frac{P_i}{\rho_i^2}\right)\nabla_i W(\mathbf{r}_i - \mathbf{r}_j, h) + \sum_j m_j \frac{(\mu_i + \mu_j)(\mathbf{v}_i - \mathbf{v}_j)}{\rho_i\rho_j(\mathbf{r}_i - \mathbf{r}_j)^2}(\mathbf{r}_i - \mathbf{r}_j)\nabla_i W(\mathbf{r}_i - \mathbf{r}_j, h) + \mathbf{g}. \tag{16}$$

The SPH approximation for the pressure gradient was derived by Gingold and Monaghan [6] and the SPH approximation for the viscous force was proposed by Morris et al. [10].

For the modified SPH model with particle masses which depend on the fluid composition, the change of momentum for particle i can be written as

$$\frac{\mathrm{d}(m_i\mathbf{v}_i)}{\mathrm{d}t} = \mathbf{F}_i, \tag{17}$$

where $\mathbf{F}_i$ is the total force acting on the particle i. This leads to the SPH equation

$$\mathbf{F}_i = -\sum_j\left(\frac{P_j}{n_j^2} + \frac{P_i}{n_i^2}\right)\nabla_i W(\mathbf{r}_i - \mathbf{r}_j, h) + \sum_j \frac{(\mu_i + \mu_j)(\mathbf{v}_i - \mathbf{v}_j)}{n_i n_j(\mathbf{r}_i - \mathbf{r}_j)^2}(\mathbf{r}_i - \mathbf{r}_j)\nabla_i W(\mathbf{r}_i - \mathbf{r}_j, h) + m_i\mathbf{g}. \tag{18}$$

By analogy, the convection-diffusion equation can be written in the form [11]

$$\frac{\mathrm{d}C_i}{\mathrm{d}t} = \sum_j \frac{(D_i n_i + D_j n_j)(C_i - C_j)}{n_i n_j(\mathbf{r}_i - \mathbf{r}_j)^2}(\mathbf{r}_i - \mathbf{r}_j)\nabla_i W(\mathbf{r}_i - \mathbf{r}_j, h). \tag{19}$$

These equations are coupled because the particle mass that appears in the momentum conservation equation changes as a consequence of diffusion. In general, both the viscosity and the relationship between the pressure and the number density also depend on the fluid composition, and hence they are influenced by diffusion. However, we assumed that both the fluid viscosity and the equation of state are independent of composition for the sake of simplicity. Because of their symmetric forms, Eqs. (8) and (17)–(19) conserve mass and linear momentum exactly.

At each time step in a simulation, the particle number densities, n_i, at each of the particles are calculated using Eq. (8) and the pressure at each particle is obtained using the equation of state

$$P = P_{\mathrm{eq}} \frac{n_i}{n_{\mathrm{eq}}}. \tag{20}$$

Then the right hand side of Eq. (19) is evaluated and new concentrations are found.

The forces acting on each particle are found from Eq. (18), and new particle velocities and particle positions are found by time integration using the explicit "velocity Verlet" algorithm [16], which takes the form

$$\begin{aligned} &\mathrm{r}_i(t+\Delta t) = \mathrm{r}_i(t) + \Delta t \mathbf{v}_i(t) + 0.5\Delta t^2 F_i(t)/m_i(t), \\ &C_i(t+\Delta t) = \left[C_i(t) + 0.5\Delta t \left\{ \frac{\mathrm{d}C_i(t)}{\mathrm{d}t} + \frac{\mathrm{d}C_i(t+\Delta t)}{\mathrm{d}t} \right\} \right], \\ &m_i(t+\Delta t) = m_i^{\mathrm{f}} + kC_i(t+\Delta t) \end{aligned} \tag{21}$$

and

$$\mathbf{v}_i(t+\Delta t) = [m_i(t)\mathbf{v}_i(t) + 0.5\Delta t\{\mathbf{F}_i(t) + \mathbf{F}_i(t+\Delta t)\}]/m_i(t+\Delta t). \tag{22}$$

To obtain a stable solution, the time step, Δt, should satisfy the conditions

$$\Delta t \leqslant 0.25h/3c, \quad \Delta t \leqslant 0.25 \min_i (h/3 \mid \mathbf{F}_i \mid)^{1/2} \quad \text{and} \quad \Delta t \leqslant \min_i (\rho_i h^2/9\mu_i),$$

where $|\mathbf{F}_i|$ is the magnitude of the force $\mathbf{F}_i$ [10].

A variety of forms, including spline functions of different order, have been used for the weighting functions. The fourth-order weighting function [11]

$$W(\mathbf{r},h) = \alpha \begin{cases} \left(3 - \frac{3|\mathbf{r}|}{h}\right)^5 - 6\left(2 - \frac{3|\mathbf{r}|}{h}\right)^5 + 15\left(1 - \frac{3|\mathbf{r}|}{h}\right)^5 & 0 \leqslant \mid \mathbf{r} \mid < h/3, \\ \left(3 - \frac{3|\mathbf{r}|}{h}\right)^5 - 6\left(2 - \frac{3|\mathbf{r}|}{h}\right)^5 & h/3 \leqslant \mid \mathbf{r} \mid < 2h/3, \\ \left(3 - \frac{3|\mathbf{r}|}{h}\right)^5 & 2h/3 \leqslant \mid \mathbf{r} \mid < h, \\ 0 & h < \mid \mathbf{r} \mid, \end{cases} \tag{23}$$

where $\alpha = \frac{63}{478\pi h^2}$ and $\alpha = \frac{81}{359\pi h^3}$ in two and three spatial dimensions, was used in this work.

The SPH approximation of the pressure gradient in (18) is based on (6), and it does not depend on the mass and density of the particle, while the original formulation of Gingold and Monaghan [7] in (16) was based on mass density and expressed in terms of m and ρ,

$$\frac{\nabla P_i}{\rho_i} = -\sum_j m_j \left(\frac{P_j}{\rho_j^2} + \frac{P_i}{\rho_i^2} \right) \nabla_i W(\mathbf{r}_i - \mathbf{r}_j, h). \tag{24}$$

It was shown by Hoover [14] that, for two-phase flow, approximation of the effects of a pressure gradient on particle velocities using Eq. (24) creates an artificial surface tension due to the jump in density at the interface between the two fluids. If the SPH formulation is based on a particle number density, which does not jump at the interface, the resulting particle equation of motion, (17) and (18), does not generated an

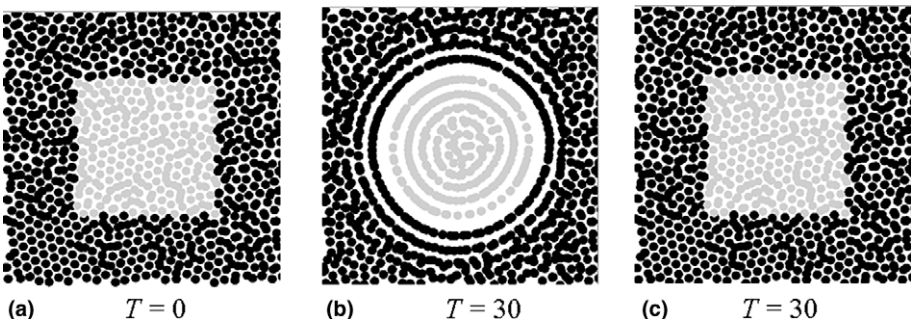

Fig. 1. Behavior of two fluids with different densities modeled with standard and modified SPH equations. (a) Initially square drop of fluid one surrounded by fluid two. (b) Standard SPH equations produce artificial surface tension resulting in transformation of the square drop into a circular drop. (c) Modified SPH equations do not create artificial surface tension, and the square shape of the fluid drop does not change.

artificial surface tension. To illustrate the difference between standard SPH and the formulation based on the number density, the behavior of an initially square droplet (at time $t = 0$, Fig. 1(a)) composed of fluid 1 surrounded by fluid 2 was simulated. Periodical boundary conditions were used in all directions. In this simulation, a diffusion coefficient of $D = 0$, was used, fluid 1 was 5 times less dense than fluid 2, and the gravitational field was set to zero. To start the simulations, particles of equal unit solvent mass and zero concentration were placed randomly into an 8 by 8 (in units of h) domain with an equilibrium particle density of $n_{eq} = 36h^{-2}$ (36 particles in an area of h^2). Then SPH equations (8), (17) and (20) were used to bring the system to an equilibrium state. In the absence of molecular diffusion ($D = 0$) the masses of particles do not change with time and Eqs. (17) and (18) can be written as

$$\frac{d\mathbf{v}_i}{dt} = -\frac{1}{m_i}\sum_j \left(\frac{P_j}{n_j^2} + \frac{P_i}{n_i^2}\right)\nabla_i W(\mathbf{r}_i - \mathbf{r}_j, h) + \frac{1}{m_i}\sum_j \frac{(\mu_i + \mu_j)(\mathbf{v}_i - \mathbf{v}_j)}{n_i n_j (\mathbf{r}_i - \mathbf{r}_j)^2}(\mathbf{r}_i - \mathbf{r}_j)\nabla_i W(\mathbf{r}_i - \mathbf{r}_j, h) + \mathbf{g}. \quad (25)$$

For single phase flow (all particles have equal constant masses) the standard and modified SPH equations are equivalent. P_{eq} in the equation of state (20) was set to 144. When the system reached equilibrium the concentration of fluid 2 particles (indicated by a black color in Fig. 1(a)) was increased from zero to 8. With $k = 0.5$ in Eq. (13) this results in a mass of $m_i = 5$ for the fluid 2 particles, while the mass of fluid 1 particles remained unity. A simulation carried out using the standard SPH equations (9) and (16) resulted in the formation of a circular droplet as a result of the artificial surface tension (Fig. 1(b)). The equation of state used in this simulation was $P_i = \rho_i/(m_i n_{eq})$ obtained from the equation of state (20) by multiplying and dividing the right hand site of (20) with m_i. When the modified SPH equations (8), (17) and (20) were used to simulate the two fluid system, the initially square droplet remained unchanged (Fig. 1(c)). This indicates that the modified SPH equations, based on the particle number density, do not generate artificial surface tension. This is particularly important for miscible flow simulations in which surface tension is not present.

3. Two-dimensional simulation of the Rayleigh–Taylor instability

In this section, the behavior of a layer of heavy fluid (salt water, for example) positioned above a layer of a light fluid (fresh water, for example) with an initially flat horizontal interface is addressed. Impermeable no-slip boundary conditions were used at the lower boundary of the computational domain, and periodic boundaries were used in the lateral directions (material leaving the right boundary enters at the left and vise-versa). Using the modified SPH equations described above, diffusion coupled with flow induced by

the action of gravity on the density variations in the fluid mixture was simulated. Fig. 2 shows the effect of the diffusion coefficient D on the development of the Rayleigh–Taylor instability. The size of the domain is 16 by 8 in units of the range, h, of the weighting function, and the equilibrium particle density was

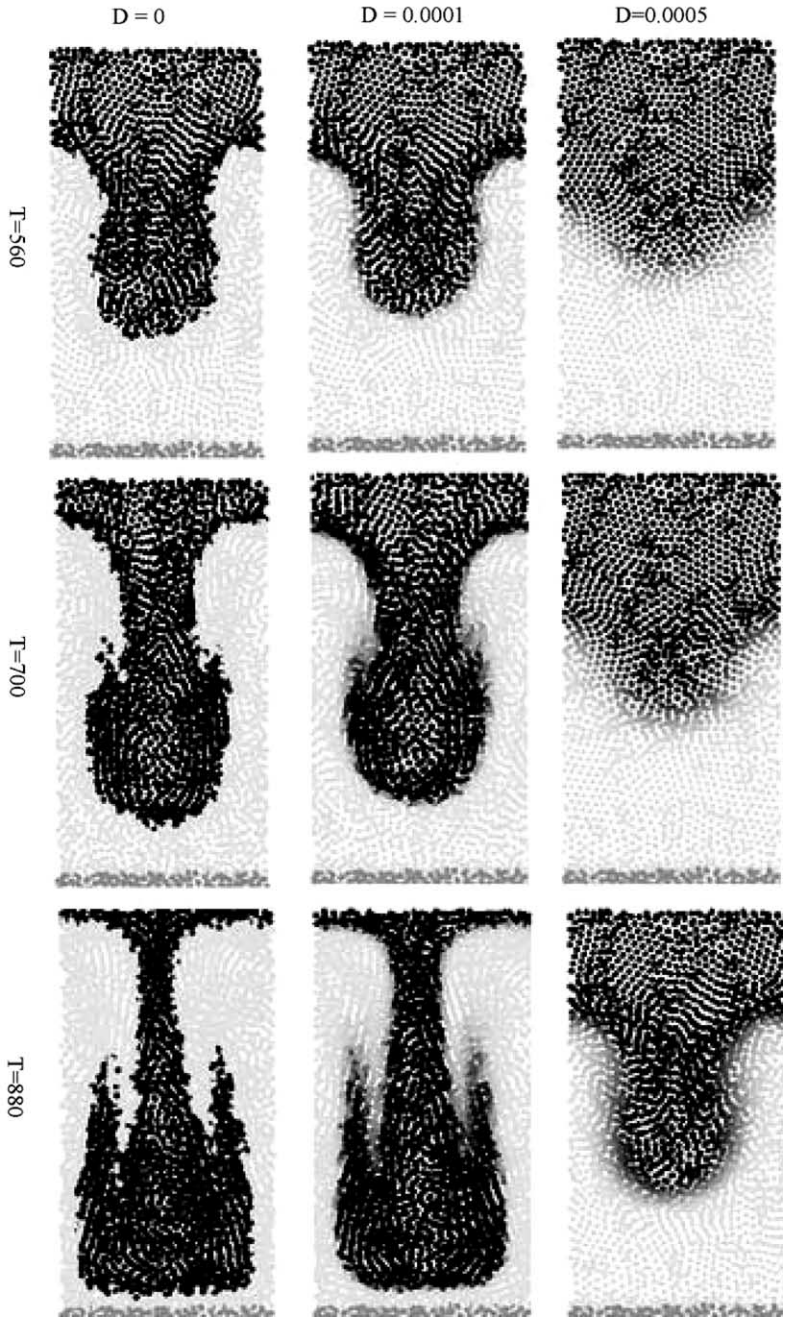

Fig. 2. Development of a two dimensional Rayleigh–Taylor instability with dimensionless time t as a function of the diffusion coefficient D. The solute concentration decreases from $C = 4$ (black) to zero concentration (light gray). The darker gray particles at the bottom are used to model the impermeable boundary.

$n_{eq} = 36h^{-2}$ (36 particles in an area of h^2). The coefficient P_{eq} in the barotropic (athermal) ideal gas equation of state was $P_{eq} = 144$ and the viscosity was $\mu = 6$. The initial solute concentration in the heavy fluid was set to $C = 4$ and the concentration of solute in the light fluid was $C = 0$. The coefficient k in expression (13) was $k = 0.5$, and the mass of solvent carried by each particle, m_i^f, was equal to unity. Consequently, the density ratio between the heavy and light fluids was 3.0, $(1 + 4 \times 0.5)$. The dimensionless acceleration due to gravity was assigned a value of $g = 0.005$. In an experiment, small deviations from an ideal horizontal interface would be unavoidable. To initiate the Rayleigh–Taylor instability in the SPH simulations, the interface between the two layers was perturbed from $y(x) = y_0$ to $y = y_0 + \sin(\pi x/8)$. In Fig. 2, the concentration C_i of the solute associated with the particles is indicated by a gray scale ranging from white for pure solvent to black for the highest solute concentration ($C = 4$). The dark gray particles at the bottom of the computational domain were used to model the impermeable lower boundary. The sinusoidal perturbation of the front grows initially into a rounded finger. As the heavy fluid accelerates downward and light fluid rises up, a Helmholtz instability develops resulting in velocity vortices, and an inverted mushroom like pattern develops. The vortices associated with the formation of an inverted mushroom shaped pattern are illustrated by the fluid velocity field shown in Fig. 3.

It can be seen that diffusion decreases the instabilities. In the absence of diffusion, a sharp interface between the high density and low density fluids is maintained, and the effects of gravity acting on density variations are not reduced by diffusion. As diffusion increases, the interface broadens and the instability becomes weaker. Results similar to those shown in Fig. 2 at a dimensionless time of $T = 560$ were reported by Fournier et al. [17] who used a spectral method to solve the two-dimensional Navier–Stokes and advective-diffusion equations (they did not report results for later times). In the absence of molecular diffusion, the SPH simulation results closely resemble those obtained by Lattice-Boltzmann simulations [18].

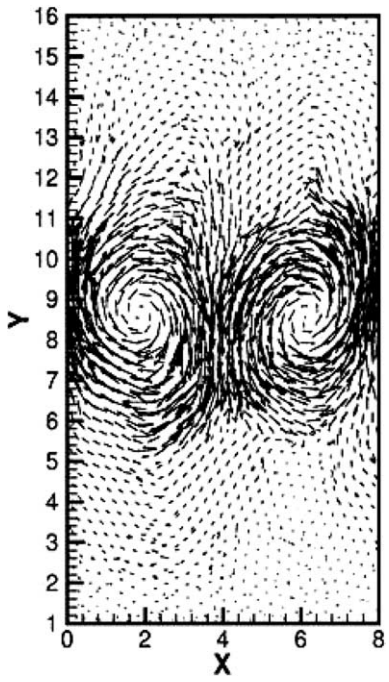

Fig. 3. Velocity field during two dimensional Rayleigh–Taylor instability at dimensional time $t = 400$. Diffusion coefficient $D = 0.0001$.

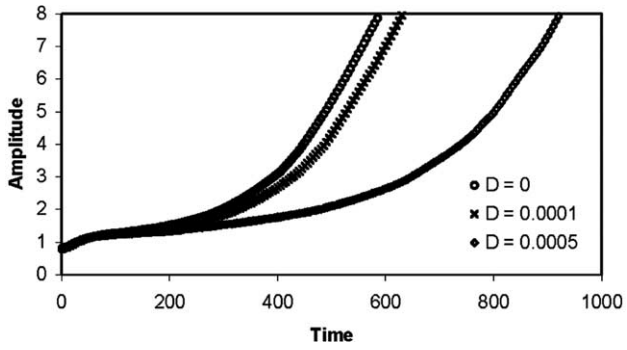

Fig. 4. Growth of the perturbation amplitude (in units of h) resulting from a two-dimensional Rayleigh–Taylor instability with dimensionless time as a function of the dimensionless diffusion coefficient D.

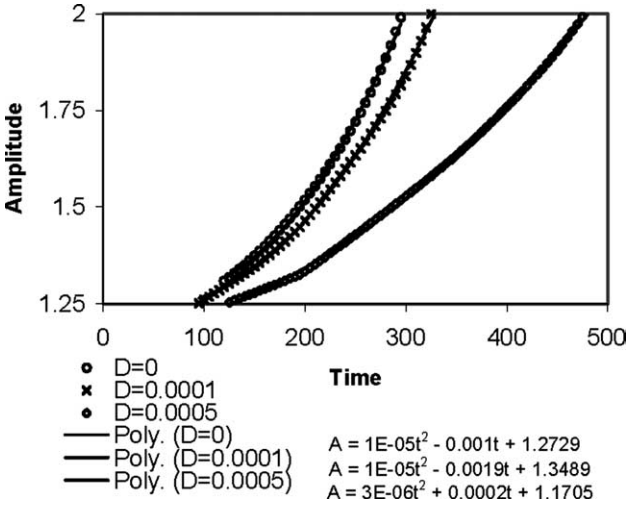

Fig. 5. Comparison of perturbation amplitude growth with the second degree polynomial growth predicted by Duff's heuristic dispersion law for different dimensionless diffusion coefficients D.

Fig. 4 shows the growth of the perturbation amplitudes as a function of time for the miscible displacements described above with three different diffusion coefficients. At early times, the initial sinusoidal perturbation is reshaped into an essentially constant form, which then grows as the square of time, in agreement with the heuristic dispersion law obtained by Duff et al. [19] from a linear stability analysis. Fig. 5 shows part of Fig. 4 for the time interval $t = 100$ to $t = 500$. It can be seen that over this time interval the growth of the amplitude A can be represented by a second order polynomial $A = A_0 + A_1 t + A_2 t^2$ (the form of the polynomials is displayed in the low right corner of Fig. 5).

4. Miscible flow in fractures

To simulate miscible flow in three-dimensional fractures the aperture geometry was generated from self-affine fractal surfaces. The fractal model is based on extensive observations that the fracture surfaces of

brittle materials, including rocks [20], have a self-affine fractal geometry [21,22], which can be characterized by a Hurst exponent with a more or less material independent (quasi-universal) value of about 0.75 [23,24]. The fracture aperture was simulated as the gap between a self-affine surface with a Hurst exponent of 0.7 and a replica of the surface, which was translated both horizontally and vertically, without rotation and with periodic boundaries in the directions parallel to the plane of the fracture. Fig. 6 shows the resulting fracture aperture field that ranges from 0 to $3.75h$ (with a gray scale ranging from white for the minimum aperture size to black for the maximum aperture) and the geometry of the fracture walls. The fracture size in the lateral directions (parallel to the plane of the fracture) was 16×16 in units of h (Fig. 7) and the (vertical) thickness of the computational domain was $16h$.

Interactions with the boundaries of the fracture were modeled using 'boundary' particles that are immobile but were included in the calculation of the total force acting on the fluid particles in Eqs. (17) and (19). Periodic boundary conditions were used in the x and y directions, parallel to the plane of the fracture. Initially particles were placed randomly in a $16 \times 16 \times 16$ box, and then the SPH equation of motion with zero gravitational acceleration was used to relax the system. Once the particles reached an equilibrium distribution, the fracture geometry was imposed on the particle system. The particles outside of the fracture aperture, within a distance h from the self-affine surfaces, were 'frozen' and labeled as boundary particles creating the fracture walls. The particles inside the fracture were left to represent the fluid and the particles outside of the fracture walls were then removed. The flow was initiated by applying a gravitational

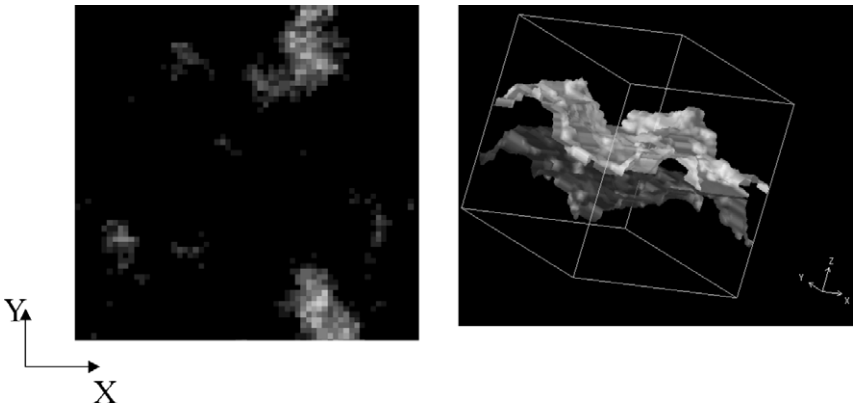

Fig. 6. Aperture size distribution (left) and geometry of a fracture walls (right). The gray scale ranges from white for the minimum aperture of zero to black for the maximum aperture of 3.75 in units of h.

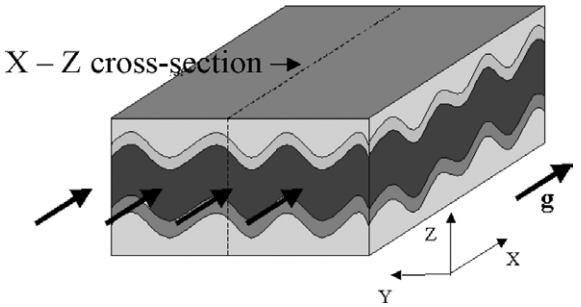

Fig. 7. Sketch of the fracture. Gravity acts in the x-direction.

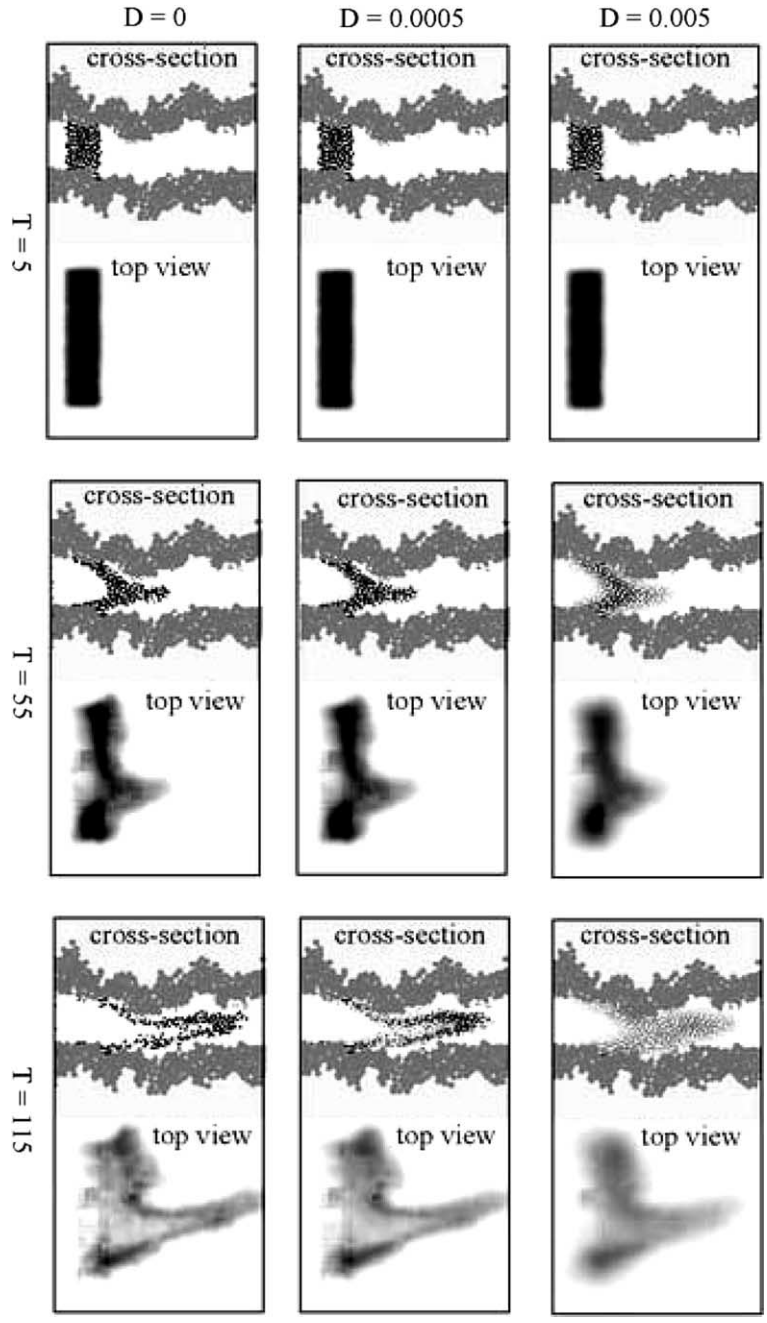

Fig. 8. Miscible flow in the fracture. The x–z cross-section and the x–y top view are shown at three different dimensionless times, t, for three different dimensionless diffusion coefficients, D. In the cross-section the small particles denote the fluid particles with non-zero solute concentration. The value of the concentration is denoted by the gray scale with black corresponding to the maximum solute concentration $C = 4$ and white to zero solute concentration. The larger gray particles are used to model impermeable fracture walls. The top view shows the concentration averaged over the plane of the fracture.

acceleration of $g = 0.01$ in direction x and periodic flow boundary conditions in directions x and y. The volume of the fracture aperture was $709h^3$ the equilibrium particle number density, n_{eq}, was 36 particles h^{-3} and the total number of mobile particles representing the fluid was 25,513.

Once a steady state flow of fluid representing the solvent was achieved, the time was set to zero and 'solute' was added to form a dense solution in a narrow zone spanning the fracture aperture near the 'entrance' to the fracture. The concentration of the solute outside the solution zone was set to zero and inside the solution zone the solute concentration was set to $C = 4$. With $k = 0.5$ this creates a density ratio of 3 between the initial solution zone and the pure solvent. The equilibrium pressure, P_{eq}, was assigned a value of 144 and a viscosity of $\mu = 3$ was used.

Fig. 8 shows the migration and diffusion of the solute in the fracture aperture for three different diffusion coefficients. Cross-sections in the direction of flow and a view of the solute concentration field averaged over the width of the fracture are shown at three different times. The values of the solute concentration are denoted by a gray scale ranging from white corresponding to pure solvent (concentration of solute $C = 0$) to black for the maximum solute concentration of 4. The cross-sections show SPH particles with different solute concentrations while the top view presents solute concentrations calculated using the weighting function according to expression (6). Fig. 9 shows how the distance between the leading edge of the 0.075 concentration isopleth and the entrance of the aperture increases with time for three different diffusion coefficients.

The solute plume reaches the end of the fracture at approximately the same time for all three diffusion coefficients. As might be expected, the spreading of the contaminated zone in the direction perpendicular to flow increases with increasing diffusion coefficient.

The SPH simulations can be used to estimate the dispersion coefficient of the fracture resulting from molecular diffusion and the non-uniform fluid velocity. The migration of solute in an ideal fracture consisting of two parallel plates was simulated (Fig. 10) to evaluate the accuracy of the SPH simulations by comparison with analytical results. A two-dimensional fracture with an aperture width of $W = 14$ in units h was filled with fluid with zero solute concentration, and a gravitational acceleration of $g = 0.001$ was applied in the direction of flow. An equilibrium particle density, n_{eq}, of 49 particles h^{-2} was used, the viscosity was set to $\mu = 8$, and periodic flow boundary conditions were used in the direction of flow. After the fluid velocity field in the fracture reached steady state, solute with a concentration of $C = 4$ was placed at the entrance of the fracture. In Eq. (13) m_i^f was set to unity and k was set to zero to give a constant uniform particle mass and a solution density independent of the solute concentration. Under steady-state flow conditions the distribution of solute averaged over the fracture aperture eventually reaches a Gaussian distribution with a variance σ^2 that increases linearly with time [5]. The growth of the variance is a result of the combined

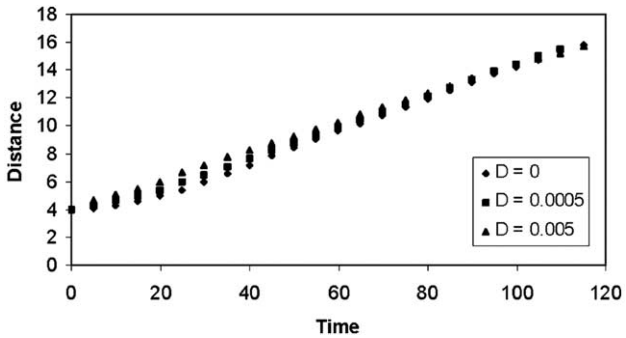

Fig. 9. Distance between the leading edge of the 0.075 concentration isopleth in the plume and the entrance of the aperture as a function of time and diffusion coefficient D.

Fig. 10. Two-dimensional simulation of Taylor–Aris dispersion, steady-state flow and transport between parallel plates. Gray scale denotes concentration distribution with black corresponding to maximum concentration and white to the zero solute concentration.

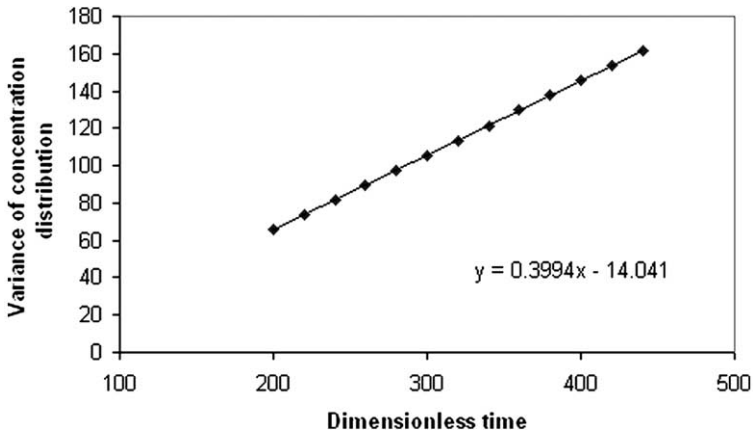

Fig. 11. Variance of concentration profile as a function of time obtained from numerical simulations (denoted by diamond symbols) and a linear fit (solid line).

effects of diffusion and advection, and the effective diffusion coefficient, known as the dispersion coefficient D^*, is larger than the true diffusion coefficient and is given by [25]

$$D* = 0.5\, \mathrm{d}(\sigma^2)/\mathrm{d}t. \tag{26}$$

According to the theory of Taylor and Aris [26] the dispersion coefficient for steady-state laminar flow between two parallel plates is given by

$$D^* = D(1 + Pe^2/210), \tag{27}$$

where $Pe = Wu/D$ is a Peclet number and $u = \rho g W^2/12\mu$ is the average velocity.

Fig. 11 shows that the variance of the solute concentration profile, σ^2, obtained from the simulations increases linearly with time with a slope of 0.399 corresponding to a dispersion coefficient of $D^* = 0.1995$ compared with a value of $D^* = 0.203$ predicted by the theory of Taylor and Aris [26].

5. Conclusion

The SPH method was modified and coupled with the advection diffusion equation to simulate the flow of miscible fluids. The model was tested by simulating the Rayleigh–Taylor instability and Taylor dispersion. According to the SPH simulation results, the Rayleigh–Taylor instability (the rate of perturbation growth) decreases with increasing diffusion coefficient. The results for a single perturbation compare well with those obtained by Fournier et al. [17], and the growth of the amplitude of the perturbation with time can be fitted fairly well by a second-degree polynomial in accord with the linear stability analysis of Duff et al. [18]. The dispersion coefficient found from SPH simulation of flow and diffusion in ideal fracture was in excellent agreement with the value predicted by the Taylor–Aris theory [26]. The SPH model was used to model three-dimensional miscible flow and transport in a fracture with complex geometry, and we are planning to use this model in future work for determination the dispersion coefficient of fractured media, a parameter used for large (field) scale simulating of contaminant transport.

Acknowledgements

This work was supported in part by the Laboratory Directed Research and Development program at the Idaho National Engineering and Environmental Laboratory (INEEL). INEEL is operated for the US DOE by Bechtel BWXT Idaho, LLC under DOE's Idaho Operations Office Contract DE-AC07-99ID13727.

References

[1] G. Taylor, The instability of liquid surfaces when accelerated in a direction perpendicular to their planes, Proc. Royal Soc. Sci. 201 (1950) 192.
[2] D.H. Sharp, An overview of Rayleigh–Taylor instability, Physica D 12 (1984) 3.
[3] J.B. Cannon, E.E. Zukoski, Turbulent mixing in vertical shafts under conditions applicable to fires in high rise buildings, Technical Fire Report No. 1 to the National Science Foundation, California Institute of Technology, Pasadena, California, 1975.
[4] R.A. Wooding, Growth of fingers at an unstable diffusing interface in a porous medium or Hele–Shaw cell, J. Fluid Mech. 39 (1969) 477.
[5] G. de Marsily, Quantitative Hydrology, Academic Press, San Diego, 1986, p. 228.
[6] L.B. Lucy, Numerical approach to the testing of the fission hypothesis, Astronom. J. 82 (1977) 1013.
[7] R.A. Gingold, J.J. Monaghan, Smoothed particle hydrodynamics:theory and application to non-spherical stars, Monthly Notices Royal Astronom. Soc. 181 (1977) 375.
[8] M.B. Liu, G.R. Liu, K.Y. Lam, Computer simulation of high explosive explosion using smoothed particle hydrodynamics methodology, Comput. Fluids 32 (2003) 305.
[9] J.J. Monaghan, Simulating free surface flows with SPH, J. Comput. Phys. 110 (1994) 399.
[10] J.P. Morris, P.J. Fox, Y. Zhu, Modeling low Reynolds number incompressible flows using SPH, J. Comput. Phys. 136 (1997) 214.
[11] Y. Zhu, P.J. Fox, J.P. Morris, A pore-scale numerical model for flow through porous media, Int. J. Numer. Anal. Meth. Geomech. 23 (1999) 881.
[12] Y. Zhu, P.J. Fox, Smoothed particle hydrodynamics model for diffusion through porous media, Transport Porous Media 43 (2001) 441.

[13] Y. Zhu, P.J. Fox, Simulation of pore-scale dispersion in periodic porous media using smoothed particle hydrodynamics, J. Comput. Phys. 182 (2002) 622.
[14] W.G. Hoover, Isomorphism linking smooth particles and embedded atoms, Physica A 260 (1998) 244.
[15] A. Colagrossi, M. Landrini, Numerical simulation of interfacial flows by smoothed particle hydrodynamics, J. Comput. Phys. 191 (2003) 448.
[16] M.P. Allen, D.J. Tildesley, Computer Simulation of Liquids, Oxford University Press, Oxford, 2001, p. 81.
[17] E. Fournier, S. Gauthier, F. Renaud, 2D pseudo-spectral parallel Navier–Stokes simulations of compressible Rayleigh–Taylor instability, Comput. Fluids 31 (2002) 569–587.
[18] X. Nie, Y. Qian, G. Doolen, S. Chen, Lattice Boltzmann simulation of the two-dimensional Rayleigh–Taylor instability, Phys. Rev. E 58 (1998) 6861.
[19] R.E. Duff, F.H. Harlow, C.W. Hirt, Effects of diffusion on interface instability between gases, Phys. Fluids 5 (1962) 417.
[20] J. Schmittbuhl, F. Schmitt, C. Scholz, Scaling invariance of crack surfaces, J. Geophys. Research-Solid Earth 100 (1995) 5953.
[21] B.B. Mandelbrot, The Fractal Geometry of Nature, W.H. Freeman, New York, 1984.
[22] B.B. Mandelbrot, D.E. Passoja, A.J. Paullay, Fractal character of fracture surfaces of metals, Nature 308 (1984) 721.
[23] E. Bouchaud, Scaling properties of cracks, J. Phys.: Condensed Matter 9 (1997) 4319.
[24] E. Bouchaud, G. Lapasset, J. Planes, Fractal dimension of fractured surfaces – a universal value, Europhys. Lett. 13 (1990) 73.
[25] A. Einshtein, Uber die von der Molecularkinetischen Theorie der Warme gefordete Bewegung von in ruhenden Flussigkeiten suspendierten Teinchen, Ann. Phys. 17 (1905) 539.
[26] R. Aris, On the dispersion of a solute in a fluid flowing through the tube, Proc. Royal Soc. 235a (1956) 67.